Thin Solid Films 520 (2012) 4031–4035

Contents lists available at SciVerse ScienceDirect

Thin Solid Films

journal homepage: www.elsevier.com/locate/tsf

# Solution-processed zinc tetrabenzoporphyrin thin-films and transistors

Patrick B. Shea [a,*], Hiroko Yamada [b], Noboru Ono [b], Jerzy Kanicki [a]

[a] Organic & Molecular Electronics Laboratory, Department of Electrical Engineering & Computer Science, The University of Michigan, Ann Arbor, MI 48109-2108, USA
[b] Graduate School of Science and Engineering, Ehime University, Bunkyo-cho 2-5, Matsuyama 790-8577, Japan

ARTICLE INFO

*Article history:*
Received 7 July 2011
Received in revised form 19 January 2012
Accepted 23 January 2012
Available online 27 January 2012

*Keywords:*
Organic transistors
Porphyrins
Precursor-route
Small molecules

ABSTRACT

Thin-films and organic field-effect transistors fabricated from a solution-processable precursor of zinc tetrabenzoporphyrin (ZnTBP) are reported. Amorphous, insulating precursor films were deposited by spin-casting and thermally converted into polycrystalline, semiconducting thin-films comprising grains on the order of 5 μm in diameter. Thin-film X-ray diffraction indicates a monoclinic unit cell with molecules arranged in a herringbone pattern, which in conjunction with optical and atomic force microscopy indicate a thin-film with grains comprised of randomly oriented ZnTBP aggregates. Optical absorption measurements display broad absorption with bands characteristic of a $D_{4h}$ symmetric porphyrin molecule. Organic field-effect transistors displayed field-effect mobilities on the order of $10^{-2}$ $cm^2/V$ s and ON-/OFF-current ratios exceeding $10^2$.


## 1. Introduction

Transition-metal porphyrins and phthalocyanines constitute vital components of ubiquitous biochemical systems [1]. Due in part to their high electrical performance and chemical stability, vapor deposited metallophthalocyanines (MPCs) have been staple organic field-effect transistor (OFET) materials during the last decade [2,3], and are increasingly appearing as both donor and acceptor layers in bulk heterojunction organic photovoltaics (OPVs) [4,5]. Zinc porphyrins in particular, due to their unique optical properties, have been utilized as an effective antenna for photosynthetic processes [6,7] and in chemically and optically sensitive molecular wires [8,9]. Zinc porphyrins are also potential materials for optoelectronic molecular devices exploiting exciton–polaron coupling for nonlinear optics and polariton lasers [10]; a zinc porphyrin was utilized in the initial demonstration of polaritons in an organic microcavity [11].

Precursor-route small molecule organic semiconductors are also the focus of intense research because they potentially harness the ease of processing allowed by solution-processable organic semiconductors while producing crystalline thin-films with high charge mobility [12–14]. The semiconductor is functionalized with a bulky side molecule that renders the small molecule soluble, which can then be removed by a thermal or optical process [15], or left in place to modify molecular ordering [16]. Precursor-route metallotetrabenzoporphyrins (MTBPs) have been demonstrated in solution-processed OFETs with field-effect mobilities in the range of $10^{-2}$–1 $cm^2/V$ s, with metallation found to induce variations in single-crystal size, polycrystallinity, and aggregation [17–20]. Precursor-route MTBPs allow solution processable device fabrication, polycrystalline and semiconducting thin-films, and thermal and chemical stability following precursor thermal conversion by a retro-Diels–Alder reaction, enabling further processing without deleterious effects on the thin-film [21]. In addition to OFETs, precursor-route TBP has been demonstrated as an effective donor film in OPV devices because of its absorption spectrum, and because the insoluble, converted film allows for significant post-processing [22,23]. Considering the small changes in the chemical synthesis process that can yield a wide array of MTBPs, this combination of electrical behavior, film morphology, and chemical tunability presents tantalizing possibilities for high performance, printable organic biochemical sensors and photovoltaics. Zn is of particular interest as the metal in a solution-processable MTBP OFET for several reasons. Solution processing is enabled using the soluble precursor, and the well-ordered molecular aggregation observed in other precursor-route MTBPs combined with the optical characteristics of Zn porphyrins may potentially induce strong exciton–polaron coupling within the active region of a transistor or other organic electronic device. In this work we report thin-films and OFETs fabricated from precursor-route zinc tetrabenzoporphyrin (ZnTBP). Thin-film X-ray diffraction, optical absorbance and microscopy, atomic force microscopy, and transistor electrical measurements are examined, and discussed relative to other MTBPs demonstrated as OFET active materials.

## 2. Experimental details

Tetrabicyclo [2,2,2]octadienporphyrin zinc complex, or zinc tetrabicycloporphyrin (ZnCP) was synthesized according to Ref. [24], and

* Corresponding author at: Advanced Concepts & Technology Development, Northrop Grumman Electronic Systems, Linthicum, MD, USA. Tel.: +1 734 936 0964; fax: +1 734 615 2843.
*E-mail address:* pshea@umich.edu (P.B. Shea).
*URL:* http://www.eecs.umich.edu/omelab (J. Kanicki).

0040-6090/$ – see front matter © 2012 Elsevier B.V. All rights reserved.
doi:10.1016/j.tsf.2012.01.034

was dissolved (0.9 wt%) in chloroform. Substrates were prepared by washing in acetone and isopropyl alcohol, followed by a 20 minute exposure to UV-ozone and a 20 minute soak in 200 prf ethanol. The precursor solution was then spun-cast in air onto the target substrate and thermally converted via a retro-Diels–Alder reaction to ZnTBP by annealing in vacuum at 180 °C for 30 minutes (Fig. 1). ZnTBP thin-films after thermal conversion were approximately 100 nm thick. Films for X-ray-diffraction (XRD) were deposited onto bare, undoped (*n*-type, 100 Ω cm, <100>) crystalline silicon substrates. XRD measurements were performed with a Bruker-AXS D8 Discover with a Cu-Kα radiation source in reflection geometry mode. Ultraviolet–visible (UV–vis) absorbance measurements were performed with a Varian-Cary 5e spectrometer for photon energies 1 eV ≤ $h\nu$ ≤ 6 eV, with the zinc complex films being spun-cast onto quartz substrates. Films for optical microscopy, atomic force microscopy (AFM), and OFETs were spun-cast onto heavily-doped crystalline silicon substrates coated with a 100 nm-thick thermal oxide layer. AFM was performed using a Veeco Dimension Icon with silicon tip in tapping mode. OFETs were completed following thermal conversion by vacuum thermal evaporation of Au (60–70 nm) through a stencil mask to form staggered source and drain electrodes. Electrical measurements were performed in air and in the dark using a Hewlett-Packard 4156A semiconductor parameter analyzer. Contact to the substrate backside gate electrode was made using conductive indium–gallium eutectic. Prior to transistor measurements, ZnTBP OFETs were isolated by scratching a moat of the ZnTBP thin-film around the device under test. P-type accumulation mode operation was observed, and the measured gate electrode current ($I_G$) was negligible compared to the drain electrode current ($I_D$). During test the source electrode was set as ground. For transfer characteristics, the gate-source potential ($V_{GS}$) was swept from the ON state to the OFF state (from −40 V to +20 V), while the drain-source potential ($V_{DS}$) was held constant; for output characteristics $V_{GS}$ was stepped from the ON state to the OFF state, while $V_{DS}$ was swept from 0 V into saturation.

## 3. Results and discussion

### 3.1. Diffraction and microscopy

Precursor ZnCP films were found to be amorphous, displaying neither visible crystallization nor diffraction peaks. The XRD pattern for spun-cast ZnTBP is shown in Fig. 2, with the substrate background signal removed. The thin-film XRD data were used to determine the ZnTBP unit cell and atomic coordinates by the Rietveld powder refinement method with Pareto optimization to minimize the potential energy [25,26]. The thin-film unit cell is monoclinic with $P2_1/n$ symmetry, with ZnTBP molecules arranged in a herringbone structure. The lattice, shown in Fig. 3, has parameters $a = 12.32$ Å, $b = 6.56$ Å, $c = 14.99$ Å, and $\beta = 101.75°$. The unit cell of ZnTBP is nearly isomorphous to the other reported solution-processed MTBPs [17,19,20,27], and the ZnTBP molecule bond lengths and angles are similar to those reported for single molecule zinc porphyrins by both experiment and calculation [28–30]. The 2θ positions of the diffraction peaks are listed for ZnTBP, CuTBP, NiTBP, and TBP in Table 1, along with the corresponding Miller indices for the respective peaks. In the case of ZnTBP, while the prevalence of diffraction peaks indicates the formation of numerous crystal planes, the equivalent, small amplitude of both small and large angle diffraction peaks suggests that the thin-films are comprised of randomly oriented crystals formed from random seed sites in the precursor film.

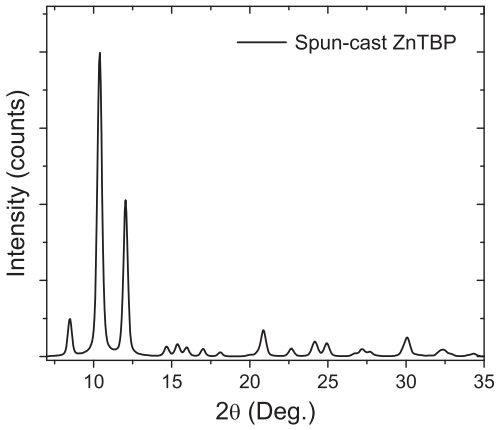


**Fig. 2.** X-ray diffraction pattern of spun-cast, solid ZnTBP.

A polarized optical micrograph of ZnTBP is shown in Fig. 4. ZnTBP thin-films are polycrystalline, with a mean grain diameter on the order of 5 μm. The grains appear petal shaped, as compared to the diamond shape reported by Noguchi et al. for CuTBP thin-film crystallization [31]. Unlike for the nickel tetrabenzoporphyrin precursor, no spontaneous crystallization of ZnCP in thick solutions or films was observed [19]. Furthermore, AFM imagery shown in Fig. 5 indicates ZnTBP does not display the millimeter-sized, randomly-ordered single crystals observed in NiTBP thin-films [19] or grains comprised of small, ordered J-aggregates displayed in CuTBP thin-films [20]. In conjunction with the display of petal shaped grains, AFM imagery indicates the grains are comprised of randomly oriented molecular aggregates, as noted in thin-films of CuTBP when heated rapidly to high temperature as compared to low temperature, wherein aggregates were found to align within the grains [20,31].

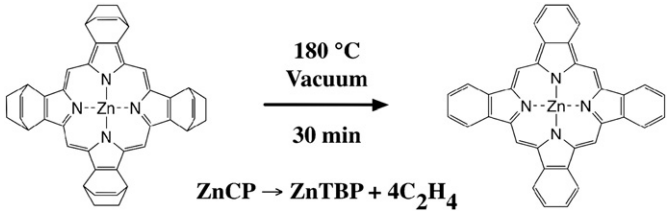


**Fig. 1.** The thermal conversion from ZnCP to ZnTBP.

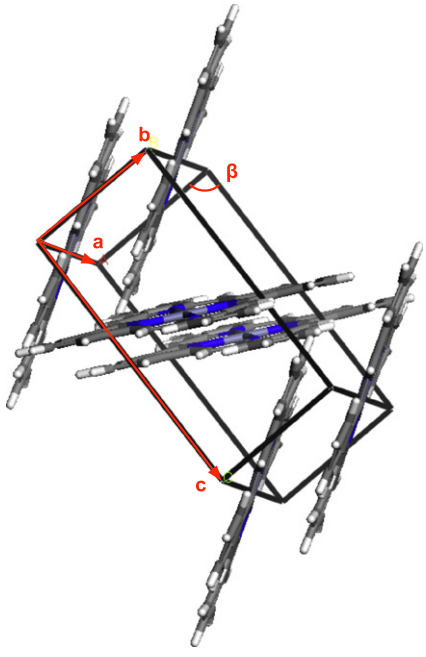


**Fig. 3.** The monoclinic ZnTBP unit cell.

**Table 1**
Comparison of 2θ diffraction peaks for TBP [27], CuTBP [20], NiTBP [19], and ZnTBP thin-films from Fig. 2, with the corresponding Miller indices.

| TBP [27] | CuTBP [20] | NiTBP [19] | ZnTBP | (hkl) |
|---|---|---|---|---|
| 8.43 | 8.51 | 8.51 | 8.50 | $10\bar{1}$ |
| 10.21 | 10.27 | 10.22 | 10.40 | 101 |
| 11.87 | 11.99 | 11.90 | 12.05 | 002 |
| 14.49 | 14.64 | 14.64 | 14.70 | 011 |
| 16.95 | 16.95 | 16.92 | 17.01 | 111 |
| 17.98 | 18.03 | 18.01 | 18.07 | 012 |
| 20.66 | 20.33 | 20.25 | 20.85 | 112 |
| 22.47 | 22.55 | 22.45 | 22.66 | 013 |
| 24.62 | 24.75 | 24.65 | 24.92 | 113 |
| 29.70 | 29.85 | 29.67 | 30.08 | 114 |

### 3.2. Optical properties

Porphyrin absorption spectra are typically comprised, in order of increasing photon energy, of moderate *Q* bands for 1.5 eV≤$h\nu$≤2.75 eV; strong Soret, or *B*, bands near $h\nu$=3 eV; strong *N* bands around $h\nu$=4 eV; and *L* and *M* bands above $h\nu$≥5 eV, where the *L* band often appears like a shoulder for the large *M* peak [1]. Peak position, width, and splitting vary due to core and peripheral substitutions, in this case Zn core metal and peripheral tetrabenzo incorporation [29]. The UV–vis absorbance spectra for spun-cast ZnCP and ZnTBP on quartz are shown in Fig. 6. Both ZnCP and ZnTBP display doublet peaks in the *Q* band indicative of the zinc complex's four-fold symmetry ($D_{4h}$) [28,29,32], with the peaks in ZnCP at 2.20 and 2.34 eV and in ZnTBP at 1.91 and 2.16 eV. Prior to thermal conversion from ZnCP to ZnTBP the doublet peaks in ZnCP display nearly equivalent absorption intensity. Following thin-film thermal conversion both peaks red-shift and the lower energy peak dominates the higher energy peak, likely indicating a reduction in the $\pi-\pi^*$ transition. In both ZnCP and ZnTBP the *B* band peak near 3.1 eV displays the strongest absorbance, whereas in thin-films of NiTBP the *M* displayed the strongest absorption [19], although following thermal conversion both the *Q* and *M* bands in ZnTBP display higher absorption relative to the *B* peak. Following thermal conversion the mean overall absorption in the measured range in increased, indicating the formation of broad and numerous allowed energy transitions. Comparatively the *Q* and *B* absorption peaks in ZnTBP are blue-shifted relative to the TBP and CuTBP thin-films [20,33,34] and slightly red-shifted relative to NiTBP [19], indicating ZnTBP thin-films have a wider optical bandgap than TBP and CuTBP and a narrower optical bandgap compared to NiTBP. Compared to the calculated and measured absorption spectra of single-molecule ZnTBP, the *Q* and *B* bands are red-shifted 0.6 eV and 0.2 eV, respectively [29,35].

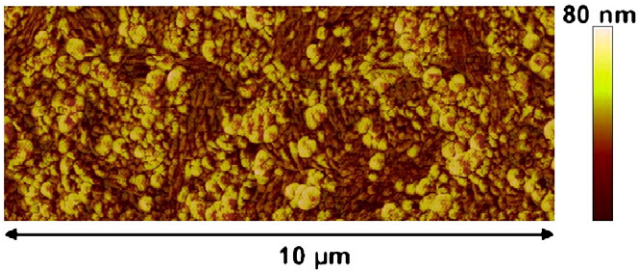


**Fig. 5.** Atomic force microscopy height image of a spun-cast ZnTBP thin-film. The *Z*-axis scale is 80 nm.

### 3.3. Transistor characteristics

The OFETs results presented here have a *W*/*L* ratio of 500 and a measured gate oxide aerial capacitance of 24.5 nF/cm$^2$. The output characteristics of such a typical ZnTBP are shown in Fig. 7. In the output characteristics, contact resistance manifests itself in nonlinear behavior of $I_D$ in the output characteristics at low $V_{DS}$. No offset in the drain current near $V_{DS}$=0 V is observed, indicating negligible gate electrode leakage current and sufficient transistor isolation. The saturation regime is distinct for smaller values of $V_{GS}$ but displays a finite output resistance.

The linear regime transfer characteristics of a typical ZnTBP OFET are shown in Fig. 8 on both a linear and semilogarithmic scale. In the linear regime ($|V_{DS}|<|V_{GS}-V_T|$) the FET gradual-channel approximation of the current–voltage relations can be described by [36,18]

$$I_D^{Lin} = -\frac{W}{L}\mu_{FE0}^{Lin} C_i (V_{GS}-V_T)^{\gamma} V_{DS} \quad (1)$$

where $\mu_{FE0}^{Lin}$ is a charge carrier field-effect mobility prefactor with units cm$^2$/V$^\gamma$ s, $C_i$ the aerial gate capacitance, $V_{GS}$ the gate-source potential, $V_T$ the accumulation threshold voltage, $V_{DS}$ the drain-source potential, and γ a nonlinear gate power term used as a measure of dispersive charge carrier transport in the thin-film [36]. The field-effect mobility can then be expressed in a $V_{GS}$-dependent relation as

$$\mu_{FE}(V_{GS}) = \mu_{FE0}^{Lin} \times (V_{GS}-V_T)^{\gamma-1} \quad (2)$$

The parameters $V_T$, $\mu_{FE0}^{Lin}$, and γ were determined by fitting Eq. (1) to the electrical data shown in Fig. 8, yielding $V_T$=−1.5 V, $\mu_{FE0}^{Lin}$=0.0076 cm$^2$/V$^\gamma$ s, and γ=1.2. By Eq. (2), $\mu_{FE}$=0.015 cm$^2$/V s at $V_{GS}$=−40 V and $V_{DS}$=−10 V. The $I_{ON}/I_{OFF}$ ratio is calculated as the quotient of $I_D$ at $V_{GS}$=−40 V and +20 V; for the OFET shown in Fig. 8 $I_{ON}/I_{OFF}$=660. The low value for γ indicates post-threshold charge transport is relatively non-dispersive compared to an amorphous

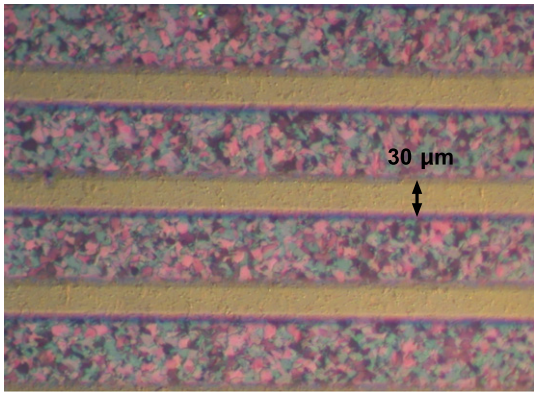


**Fig. 4.** A polarized optical micrograph of a spun-cast ZnTBP thin-film on $SiO_2$. The electrode width is 30 μm.

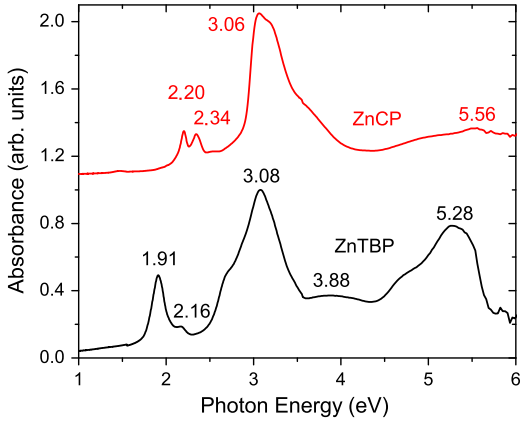


**Fig. 6.** Optical absorbance spectra of spun-cast, solid ZnCP and ZnTBP on quartz.

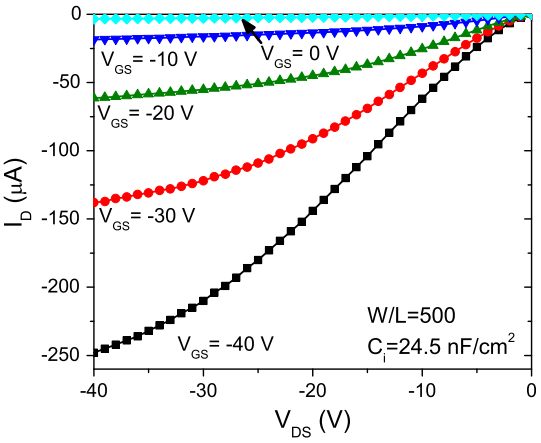


**Fig. 7.** Output characteristics of a typical ZnTBP OFET.

polymer OFET [37], and is similar to values reported for TBP and NiTBP [18,19]. However, the subthreshold slope ($S$) was measured to be 10 V/dec (Fig. 8, dashed line), indicating sub-$V_T$ charge transport is governed by mid-gap trap states, likely located at the gate insulator–semiconductor interface or within grain boundaries in the randomly oriented aggregates indicated by thin-film XRD (Fig. 2) and AFM (Fig. 5). The subthreshold slope can be related to the surface trap states, $N_{ss}$ ($cm^{-2}$ $eV^{-1}$) and the bulk trap states, $N_{bs}$ ($cm^{-3}$ $eV^{-1}$), by [38]

$$S = \frac{kT}{q\ \log(e)} \times \left[1 + C_i\left(\sqrt{\epsilon_s N_{bs} + qN_{ss}}\right)\right] \quad (3)$$

where $k$ is Boltzmann's constant, $T$ the temperature, $q$ the electronic charge, and $\epsilon_s$ the semiconductor permittivity. The permittivity of solid ZnTBP is unknown; furthermore, in solution processed TBP OFETs it has been proposed that the density of surface trap states is significantly higher than the density of bulk trap states ($N_{bs} \ll N_{ss}$) [39]. Thus, the maximum $N_{ss}$ approaches $2.42\times10^{13}$ $cm^{-2}$ $eV^{-1}$. Comparatively, in pristine TBP $N_{ss}^{max} = 2.9\times10^{12}$ $cm^{-2}$ $eV^{-1}$ [18], and in NiTBP $N_{ss}^{max} = 1.88\times10^{13}$ $cm^{-2}$ $eV^{-1}$ [19].

Comparatively, metal-free TBP OFETs demonstrated $\mu_{FE}$ similar to that observed here [17,18]. However, the OFF-state leakage current and $S$ are higher in ZnTBP than in TBP. NiTBP and CuTBP OFETs demonstrated $\mu_{FE}$ exceeding $10^{-1}$ $cm^2$/V s, as well as higher $S$ and OFF-state leakage than TBP (but lower than for ZnTBP) [19,20]. Elemental analysis found no evidence of excess metal in the ZnCP precursor, and thin-film

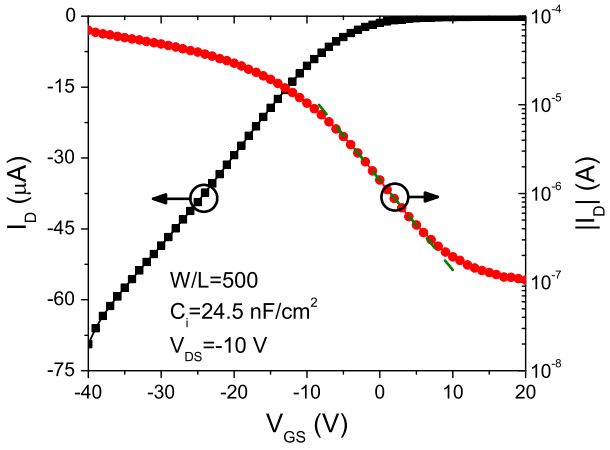


**Fig. 8.** Linear regime transfer characteristics of a typical ZnTBP OFET. The dashed line indicates the subthreshold slope calculation.

XRD does not indicate altered molecular packing. The large $S$ indicates that ZnTBP has a high density of trap states localized within the grain boundaries observed in the presented microscopy results, resulting from the random crystallization orientation displayed in the XRD patterns and AFM imagery (Fig. 5). Molecular orbital calculations and charge transport measurements of one-dimensional stacks of porphyrins and phthalocyanines indicated core-metals with open 3*d* shells (such as Cu and Ni) contribute to intermolecular charge conduction, whereas closed-shell metal 3*d* orbitals such as Zn do not contribute to charge conduction [40–42], suggesting that the increased OFF-state current is likely induced by the high density of grain boundary trap states. While the electrical behavior of ZnTBP *vis-à-vis* field-effect mobility is notably lesser than for CuTBP and NiTBP, the prevalence of Zn porphyrins in biochemistry could make it an intriguing choice for medical applications requiring sensitive lead and iron detection. For example, zinc protoporphyrin is the immediate precursor to the formation of heme, and is prevalent in the bloodstream in medical cases of excess lead or lack of iron [1,43]. Furthermore, combined with such known chemical and optical sensitivities of metal porphyrins, the high density of trap states localized in large grain boundary regions could potentially be exploited for biochemical sensing applications in chemiresistors [44] or transistors [45,46].

## 4. Conclusions

We have reported solution-processed zinc tetrabenzoporphyrin thin-films and transistors. ZnTBP films display a polycrystalline morphology following thermal conversion from an amorphous precursor film. The unit cell is isomorphous to other solution-processed metallotetrabenzoporphyrins, and displays optical absorption spectra characteristic of a $D_{4h}$ symmetric porphyrin. Morphology studies indicate thin-films are comprised of grains of 5 μm in diameter, within which ZnTBP aggregates are randomly oriented. Transistor measurements showed charge carrier field-effect mobilities around $10^{-2}$ $cm^2$/V s, with ON-/OFF-current ratios exceeding $10^2$ and threshold voltages of −1.5 V.

## References

[1] K.M. Kadish, K.M. Smith, R. Guilard (Eds.), The Porphyrin Handbook, Academic Press, 2002.
[2] Z. Bao, A.J. Lovinger, A. Dodabalapur, Adv. Mater. 9 (1997) 42.
[3] S. Liu, W.M. Wang, A.L. Briseno, S.C.E. Mannsfeld, Z. Bao, Adv. Mater. 21 (2009) 1217.
[4] I. Bruder, J. Schöneboom, R. Dinnebier, A. Ojala, S. Schäfer, R. Sens, P. Erk, J. Weis, Org. Electron. 11 (2010) 377.
[5] A. Opitz, J. Wagner, W. Bruetting, A. Hinderhofer, F. Schreiber, Phys. Status Solidi A 206 (2009) 2683.
[6] S. Prathapan, T. Johnson, J. Lindsey, J. Am. Chem. Soc. 115 (1993) 7519.
[7] F. D'Souza, P. Smith, M. Zandler, A. McCarty, M. Itou, Y. Araki, O. Ito, J. Am. Chem. Soc. 126 (2004) 7898.
[8] R. Wagner, J. Lindsey, J. Am. Chem. Soc. 116 (1994) 9759.
[9] R. Wagner, J. Lindsey, J. Seth, V. Palaniappan, D. Bocian, J. Am. Chem. Soc. 118 (1996) 3996.
[10] R. Holmes, S. Forrest, Org. Electron. 8 (2007) 77.
[11] D. Lidzey, D. Bradley, M. Skolnick, T. Virgili, S. Walker, D. Whittaker, Nature 395 (1998) 53.
[12] A.R. Brown, A. Pomp, D.M. de Leeuw, D.B.M. Klaasen, E.E. Havinga, J. Appl. Phys. 79 (1996) 2136.
[13] P.T. Herwig, K. Müllen, Adv. Mater. 11 (1999) 480.
[14] A. Afzali, C.D. Dimitrakopoulos, T.L. Breen, J. Am. Chem. Soc. 124 (2002) 8812.
[15] H. Yamada, T. Okujima, N. Ono, Chem. Commun. (2008) 2957.
[16] S. Park, T. Jackson, J. Anthony, D. Mourey, Appl. Phys. Lett. 91 (2007) 063514.
[17] S. Aramaki, Y. Sakai, N. Ono, Appl. Phys. Lett. 84 (2004) 2085.
[18] P.B. Shea, J. Kanicki, N. Ono, J. Appl. Phys. 98 (2005) 014503.
[19] P.B. Shea, L.R. Pattison, M. Kawano, J. Kanicki, P. Petroff, H. Yamada, N. Ono, J. Appl. Phys. 100 (2006) 034502.
[20] P.B. Shea, L.R. Pattison, J. Kanicki, P. Petroff, M. Kawano, H. Yamada, N. Ono, Synth. Met. 157 (2007) 190.
[21] P. Shea, J. Kanicki, Y. Cao, N. Ono, Appl. Phys. Lett. 87 (2005) 173506.
[22] M. Guide, X.-D. Dang, T.-Q. Nguyen, Adv. Mater. 23 (2011) 2313.
[23] S.-Y. Ku, C.D. Liman, J.E. Cochran, M.F. Toney, M.L. Chabinyc, C.J. Hawker, Adv. Mater. 23 (2011) 2289.
[24] Y. Shimizu, Z. Shen, T. Okujima, H. Uno, N. Ono, Chem. Commun. (2004) 374.

[25] R.A. Young, The Rietveld Method, IUCr Monographies of Crystallography, 5, Oxford University Press, 1993.
[26] D.A. Van Veldhuizen, G.B. Lamont, Evol. Comput. 8 (2000) 125.
[27] S. Aramaki, J. Mizuguchi, Acta Crystallogr. Sect. E E59 (2003) o1556.
[28] L. Edwards, M. Gouterman, C.B. Rose, J. Am. Chem. Soc. 98 (1976) 7638.
[29] K.A. Nguyen, R. Pachter, J. Chem. Phys. 114 (2001) 10757.
[30] M.-S. Liao, S. Scheiner, J. Chem. Phys. 117 (2002) 205.
[31] N. Noguchi, A. Ohno, S. Aramaki, H. Asatani, M. Matsuoka, J. Chem. Eng. Jpn. 42 (2009) 381.
[32] M. Gouterman, J. Mol. Spectrosc. 6 (1961) 138.
[33] S. Aramaki, Y. Sakai, R. Yoshiyama, K. Sugiyama, N. Ono, J. Mizuguchi, Proc. SPIE 5522 (2004) 27.
[34] P.B. Shea, A.R. Johnson, J. Kanicki, N. Ono, IEEE Trans. Electron Devices 52 (2005) 1497.
[35] K.A. Nguyen, R. Pachter, J. Chem. Phys. 118 (2003) 5802.
[36] G. Merckel, A. Rolland, Solid State Electron. 39 (1996) 1231.
[37] M.C. Hamilton, S. Martin, J. Kanicki, Chem. Mater. 16 (2004) 4699.
[38] A. Rolland, J. Richard, J.P. Kleider, D. Mencaraglia, J. Electrochem. Soc. 140 (1993) 3679.
[39] K. Seidel, M. Koehler, Phys. Rev. B 78 (2008) 235308.
[40] J. Martinsen, L.J. Pace, T.E. Phillips, B.M. Hoffman, J.A. Ibers, J. Am. Chem. Soc. 104 (1982) 83.
[41] F.W. Kutzler, D.E. Ellis, J. Chem. Phys. 84 (1986) 1033.
[42] N. Ishikawa, J. Porphyrins Phthalocyanines 5 (2001) 87.
[43] A. Lamola, T. Yamane, Science 186 (1974) 936.
[44] F. Bohrer, C. Colesniuc, J. Park, M. Ruidiaz, I. Schuller, A. Kummel, W. Trogler, J. Am. Chem. Soc. 131 (2008) 478.
[45] L. Wang, D. Fine, A. Dodabalapur, Appl. Phys. Lett. 85 (2004) 6386.
[46] T. Someya, A. Dodabalapur, J. Huang, K. See, H. Katz, Adv. Mater. 22 (2010) 3799.